Research Square

Preprints are preliminary reports that have not undergone peer review.
They should not be considered conclusive, used to inform clinical practice,
or referenced by the media as validated information.

Satellites of Broucke's prograde family R in the equal-mass planar three-body problem: periodic orbits at the rotation numbers 1/n in two reversing-symmetry classes

Utshob Kandel

utshobkandel@gmail.com

Unaffiliated

Research Article

Keywords: Periodic orbits, Three-body problem, Broucke–Hadjidemetriou–Hénon family, Satellites, Linear stability, Reversing symmetry

Posted Date: November 23rd, 2026

DOI: https://doi.org/10.21203/rs.3.rs-11425150/v1

License: This work is licensed under a Creative Commons Attribution 4.0 International License.
Read Full License

Additional Declarations: No competing interests reported.

Satellites of Broucke's prograde family R in the equal-mass planar three-body problem: periodic orbits at the rotation numbers $1/n$ in two reversing-symmetry classes

Utshob Kandel[1*]

[1*]Unaffiliated, Chitwan, Nepal.

Corresponding author(s). E-mail(s): utshobkandel@gmail.com;

Abstract

Satellites leave the family R of Broucke, the prograde branch of the Broucke–Hadjidemetriou–Hénon family of the equal-mass planar three-body problem, at branch points among its members with upper rotation number $\mathbf{1/n}$. In class C (reflection symmetry) the satellite curve of each such member ends at a periodic orbit, stored with 30 digits, for every $\boldsymbol{n}$ from 5 to 56. At the end orbits the resonant pair (at $+1$ at the branch point) is on the unit circle for $\boldsymbol{n = 5}$ to 20; the transverse pair is on it for $\boldsymbol{n \leq 12}$, so the orbits are spectrally stable, and real negative from $\boldsymbol{n = 13}$, so they are unstable. A second family (class I, a second reversing symmetry) leaves the same branch points for $\boldsymbol{n = 5}$ to 20 and ends at different orbits, with a real positive resonant pair and a transverse pair off the unit circle from $\boldsymbol{n = 13}$. Along the curves, for $\boldsymbol{n = 6}$ to 20, the type of the resonant pair, where it can be read, is opposite to that at the end orbit and changes once, at nearly the same scale-free angular momentum in both classes; near the branch point the type could not be determined. For $\boldsymbol{n = 13}$ to 20 the transverse pair passes through $\boldsymbol{-1}$ once per curve, before the end orbit. Hénon's relation gives the period correction as an angular-momentum integral. Apart from the atlas entry for $\boldsymbol{n = 7}$, none was found in the sources checked.

Keywords: Periodic orbits, Three-body problem, Broucke–Hadjidemetriou–Hénon family, Satellites, Linear stability, Reversing symmetry

1 Introduction

1.1 The problem and the BHH family

Three bodies of equal mass attract each other by Newtonian gravity, and the motion is planar. Thousands of periodic orbits with zero angular momentum have been reported (Šuvakov and Dmitrašinović 2013; Li and Liao 2017; Hristov and Hristova 2024; Hristov et al. 2024); one of them can start a family with non-zero angular momentum, but for few have such families been followed. The hierarchical families with non-zero angular momentum, in which two bodies form a binary and the third moves around it, were found by Broucke (1975), Hadjidemetriou (1975) and Hénon (1976), and are called the Broucke–Hadjidemetriou–Hénon (BHH) family; related families were also computed by Hénon (1974) and Hadjidemetriou (1976). Broucke (1975) found two families that start with the three bodies on a line and all velocities perpendicular to it, A and R. The orbits of A are retrograde (binary and outer orbit revolve in opposite directions); those of R are prograde, or direct.

1.2 Satellites and rotation numbers

An orbit of the family returns to the same shape after one relative period, turned by a rotation angle θ; it is periodic when $\theta = 0$. A member has rotation numbers ν, the fractions of a turn by which a small disturbance turns in each relative period. Where $\nu = 1/n$, the n-fold repeat of the member is degenerate (a double multiplier $+1$), and a second curve of solutions may cross the curve of repeats there; whether it does has to be found for each member (Section 2.3). The pair of nontrivial multipliers that produces the double multiplier is called the resonant pair, and the other nontrivial pair the transverse pair (Section 2.5). The orbits on this second curve are called satellites (in the older literature, bifurcations). Followed to $\theta = 0$, a satellite curve reaches a periodic orbit.

Satellites at the rotation numbers $1/n$ are the places where further families branch off a known family. At large n these branch points are near-hierarchical members of R, and whether this connects to resonant hierarchical families was not examined (Section 6.2).

1.3 What was known about satellites in general

According to Janković and Dmitrašinović (2016), one satellite of the BHH family was known before their paper, in the tables of Davoust and Broucke (1982). Janković and Dmitrašinović (2016) report 57 satellites of retrograde BHH orbits with the topological exponent k from 3 to 58, and Janković et al. (2020) (Computer Physics Communications; their tables of satellites are called the CPC tables below) about 100, up to $k = 84$. A satellite is an orbit whose topology is the k-th power of that of its progenitor. On their number, Janković et al. (2020) write that there was no known reason why it ought to be limited and that the Birkhoff–Lewis theorem (Birkhoff and Lewis 1934) says the opposite; Dmitrašinović et al. (2018) had related the existence of satellites of orbits with zero angular momentum to the stability of the progenitor by this theorem.

In their open questions they note that satellites had been observed only in the stable region of the progenitor curve, that according to Dmitrašinović et al. (2018) and the Birkhoff–Lewis theorem even linear stability may lead to infinitely many satellite orbits, and that this conjecture "would be good to verify".

1.4 What was known about the direct branch

Davoust and Broucke (1982) followed the stability and bifurcations of their families, among them D1, which is Broucke's R, up to the multiplicity three. Janković and Dmitrašinović (2016) state that the prograde satellites had not been studied systematically, and that four had been found almost inadvertently, a task that ought to be completed. Janković et al. (2020) report two preliminary searches (at $L = 0.935549$ and $L = 1.5$) with six satellites, some retrograde and some direct, and say that prograde orbits are unstable at the angular momenta searched, which makes them unlikely to have satellites by the Birkhoff–Lewis theorem, and that further searches at higher angular momentum ought to be made. These two values of L are not values of L^* and cannot be converted to it without the energy of each orbit (Online Resource 1, A.18).

1.5 What remained open, and what this paper adds

What remained open, according to the open questions of Janković et al. (2020, Section 6.1), includes whether the prograde orbits have satellites at higher angular momentum than searched there, how many satellites there are for each k, and how the existence of satellites is related to the stability of the progenitor.

Branching of orbits of period n at the members with rotation number $1/n$ is the generic behaviour known for area-preserving maps (Meyer 1970; for reversible maps, Rimmer 1980); these results do not cover the four-dimensional reduced map of this problem. What this paper contributes is therefore computational: the satellite orbits for every $n = 5$ to 56 in class C and $n = 5$ to 20 in class I, their stability, the elliptic–hyperbolic split of the resonant pair at the end orbits, and where along the curves the pairs change type.

This paper follows the satellite curve of each member of R with the upper rotation number $1/n$, $n = 5$ to 56, to $\theta = 0$ and gives the periodic orbit at its end, stored with 30 digits (the closures are in Section 3.1). The sequence bears on the remark of Dmitrašinović et al. (2018) in a limited way: the members of R used are on its linearly stable stretch, at L^* between 2.59 and 4.08, above the values of the preliminary searches, and for each of 52 values of n the satellite curve of the member reaches $\theta = 0$ at a periodic orbit. This is numerical evidence that linearly stable orbits of the direct branch have satellites at these resonances; it does not verify the remark, which is a general statement, and nothing was computed for members that are not linearly stable.

Section 5.5 states what was and what was not found in the sources checked. Part of the family was found before: the orbit for $n = 7$ is an entry of the Three Body Orbits atlas (), and one rotating member of a satellite curve is among the preliminary orbits mentioned by Janković et al. (2020) (Section 5). The sources checked are described in Section 6.3.

2 Methods

2.1 Setup and symmetric orbits

The three bodies, indexed 0, 1 and 2, have equal masses and $G = m = 1$; the orbits are planar and are integrated in double precision with a Dormand–Prince method (relative tolerance 1×10^{-13}, absolute 1×10^{-14}). With the positions $\mathbf{r}_i = (x_i, y_i)$ and the velocities $\mathbf{v}_i$, the energy and the angular momentum are

$$E = \tfrac{1}{2} \sum_i |\mathbf{v}_i|^2 - \sum_{i<j} \frac{1}{|\mathbf{r}_i - \mathbf{r}_j|}, \qquad L = \sum_i (x_i v_{y,i} - y_i v_{x,i}), \tag{1}$$

and orbits of different size are compared through the scale-free period and angular momentum

$$T^* = T\,|E|^{3/2}, \qquad L^* = |L|\,|E|^{1/2}. \tag{2}$$

The table of notation is Table 1.

The equations of motion are invariant under rotations, under the exchange of two bodies (the masses are equal) and under the reversal of time. An involution of the phase space that takes every orbit to an orbit run backwards in time is a reversing symmetry (Devaney 1976); here the reflection of the plane in a line, together with the reversal of the velocities, is one for every line, and the same combined with an exchange of bodies is another. An orbit that contains a state fixed by a reversing symmetry is symmetric, and its states at the times s and $-s$ are images of each other. The continuation of symmetric periodic orbits of reversible systems along their families is treated by Muñoz Almaraz et al. (2007).

A symmetric periodic orbit meets the fixed set of the reversing involution exactly twice in a prime period (Devaney 1976, pp. 92 and 96). A search that starts at a symmetric state and asks for the next one, half a period later, therefore finds the same orbit from either of its two symmetric states. Devaney also treats the parity of the period and the families of symmetric periodic orbits (Online Resource 1, A.14). Whether odd and even n differ is therefore a fair question; the results for $n = 5$ to 20 show no difference (Section 3.3).

The collinear–perpendicular symmetry. In the perpendicular start the bodies are on the x axis and all velocities are along y,

$$\begin{gathered} \mathbf{r}_0 = \left(-1 - \tfrac{\lambda}{3}, 0\right), \quad \mathbf{r}_1 = \left(\tfrac{2\lambda}{3}, 0\right), \quad \mathbf{r}_2 = \left(1 - \tfrac{\lambda}{3}, 0\right), \\ \mathbf{v}_0 = (0, u_1), \quad \mathbf{v}_1 = (0, u_2), \quad \mathbf{v}_2 = (0, -u_1 - u_2), \end{gathered} \tag{3}$$

so that the bodies are at -1, λ and 1 before the centre of mass is shifted to 0. This state is fixed by the reflection S in the x axis with the velocities reversed, $(x, y, v_x, v_y) \to (x, -y, -v_x, v_y)$ for each body: the symmetric states of S are the collinear states with all velocities perpendicular to the line. If the bodies are again on such a line after a time t, the orbit is symmetric under S, with symmetric states at 0 and t, and it returns to its start after the relative period $T = 2t$, turned by an angle. The rotation angle θ is that of the rotation which takes the end state of one relative period best onto the start state,

$$\theta = \operatorname{atan2}\left(\Sigma_\times, \Sigma_\cdot\right), \qquad \Sigma_\cdot = \sum_a \mathbf{a}\cdot\mathbf{b}, \qquad \Sigma_\times = \sum_a \mathbf{a}\times\mathbf{b}, \qquad \rho = \frac{\theta}{2\pi}, \tag{4}$$

where **a** and **b** run over the three positions and the three velocities of the end state and of the start state, and ρ is the rotation in turns; the orbit itself is turned by $-\theta$ in one relative period, and it is periodic when $\theta = 0$.

The isosceles symmetry of R. The orbits of R have more symmetry than S, as checked on the stored orbits. The state at the time t is the start state with bodies 1 and 2 exchanged and turned by an angle φ, $z(t) = \Gamma z(0)$, with Γ the exchange followed by the rotation by φ, and $\theta = -2\varphi$ for the relative period $2t$. Over the 242 stored points the half period state, written again as a perpendicular start, equals the original start to 7×10^{-8} at most in the start parameters (u_1, u_2, λ, t), and the deviation of the state at t itself is at most 3.81×10^{-6} in the state space (Online Resource 1, A.14). Γ is a symmetry of the equations, $S' = \Gamma S$ is another reversing symmetry and an involution, and the states at a quarter and at three quarters of the relative period are its symmetric states, which are isosceles (the derivation is in Online Resource 1, A.14). On the 242 stored points this isosceles test, with body 0 as the apex, holds at a quarter and at three quarters of the relative period, with errors at most 1.2×10^{-8} in the positions and 2.5×10^{-9} in the velocities (Online Resource 1, A.14). The derivation uses two numerical facts about R, $z(t) = \Gamma z(0)$ and the symmetry of the start under S, both as checked on the stored orbits. An orbit with these two symmetries is doubly symmetric in the sense of Muñoz Almaraz et al. (2007, Definition 8), with $R_0 = S$ at $s = 0$ and $R_1 = S'$ at $s = t/2$, and their Lemma 9 then gives $z(t + s) = S'S\, z(s) = \Gamma z(s)$, the half-period relation used here. That the members of R have these symmetries is, as above, a fact checked on the stored orbits (the lemma relates the symmetries and does not show that R has them).

Two classes. There are therefore two classes of symmetric orbits near the n-fold repeat of a member of R: the orbits symmetric under S (class C, collinear), and those symmetric under S' (class I, isosceles). Class I orbits start from the isosceles state

$$\mathbf{r}_0 = (1, 0), \quad \mathbf{r}_{1,2} = \left(-\tfrac{1}{2}, \pm\eta\right), \qquad \mathbf{v}_0 = (0, w), \quad \mathbf{v}_1 = \left(p, -\tfrac{w}{2}\right), \quad \mathbf{v}_2 = \left(-p, -\tfrac{w}{2}\right); \tag{5}$$

after the time t the state is again isosceles, with the axis turned, and the orbit is periodic when the axis returns, which is $\theta = 0$. Orbits of both classes are shown in Fig. 1.

2.2 The family R and its members with $\nu = 1/n$

The family R was traced from an orbit with $T^* = 3.7495$ and rotation angle $2/9$ turn, in both directions; the trace has 242 accepted steps. At each step the relative monodromy matrix is computed (Online Resource 1, A.14); the four eigenvalues closest to 1 count as trivial, and the others are written as modulus times $\exp(\pm 2\pi i\nu)$, with ν the rotation number,

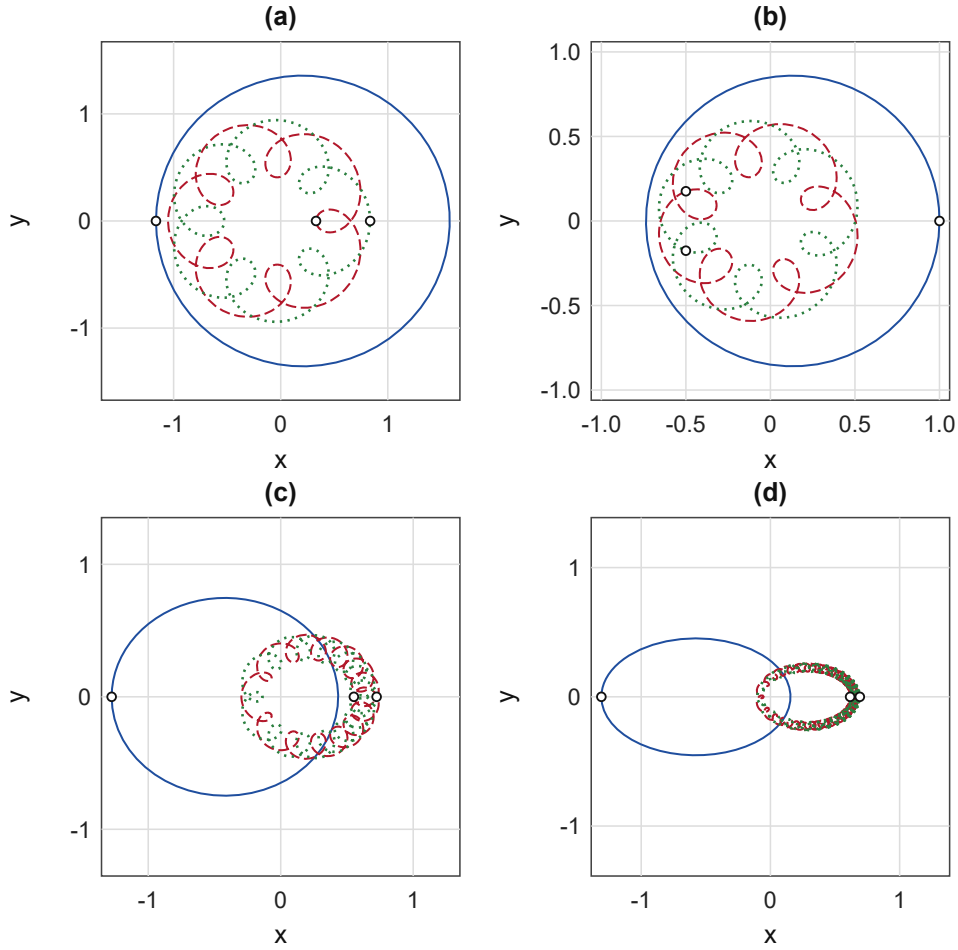


Fig. 1 End orbits ($\theta = 0$) of the satellite curves in the inertial frame over one relative period, centre of mass at the origin, equal axes: (a) class C, $n = 5$ ($T^* = 17.8468$); (b) class I, $n = 5$ ($T^* = 17.8468$); (c) class C, $n = 13$ ($T^* = 32.6398$); (d) class C, $n = 56$ ($T^* = 105.8458$). Body 0: full line (blue), body 1: dashed (red), body 2: dotted (green); the circles mark the start state, collinear for class C and isosceles for class I. The orbits close to 6.4×10^{-9} or better after one relative period (double precision integration from the 30-digit starts). In panel (d) the paths of bodies 1 and 2 form a dense band whose loops cannot be told apart at this size.

$$\mu = |\mu|\, e^{\pm 2\pi i \nu}, \qquad \nu \in [0, \tfrac{1}{2}]. \tag{6}$$

On the stable stretch a member has two rotation numbers, the lower ν_{lo} and the upper ν_{up}. A member with $\nu_{\mathrm{up}} = 1/n$ is found by bracketing and bisection, and closed by multiple shooting (Online Resource 1, A.19). At such a member the n-fold repeat is degenerate: its relative monodromy matrix has a double multiplier $+1$ besides the trivial ones. This makes the member a candidate branch point and does not by itself

Table 1 Notation.

symbol	meaning
$\mathbf{r}_i$, $\mathbf{v}_i$, E, L	position and velocity of body $i = 0, 1, 2$; energy and angular momentum, eq. (1)
T^*, L^*	scale-free period and angular momentum, eq. (2)
$T = 2t$	relative period; t is the time between two symmetric states
θ, ρ	rotation angle (end state onto start state) and rotation in turns, $\rho = \theta/2\pi$, eq. (4)
λ, η, Λ	family parameter of the start: λ in class C, eq. (3); η in class I, eq. (5); Λ either of them
u_1, u_2; p, w	the other start variables of class C and of class I
S, S', Γ	reversing symmetries ($S' = \Gamma S$) and the exchange of bodies 1 and 2 followed by a rotation by φ
n	the integer with $\nu = 1/n$ (a label of the member, not a parameter); also the number of the end orbit
ν, ν_{lo}, ν_{up}	rotation number of a member of R, eq. (6), and its lower and upper value
j	numerator of a rotation number j/n
k	topological exponent: the satellite has the topology of the k-th power of its progenitor
q	number of pieces of a multiple shooting
α_r, α_t	angles (turns) of the resonant and of the transverse pair of multipliers on the unit circle
μ_r, μ_t	moduli of the resonant and of the transverse pair when it is real
Ψ_τ, $\mathbf{f}$, $\mathbf{g}$, W	flow over the time τ; vector field; generator of the rotation; subspace of eq. (9)
F, Z, J	shooting residual, unknowns and Jacobian, eq. (7)
δ_n, ε_n	correction of the period and excess of the n-fold repeat, Section 4.1

give a second branch (Section 2.3). The stored trace has crossings of the upper $\nu = 1/n$ for n up to 58; Section 3.4 extends it.

2.3 Branch points, satellite curves and zeros

The n-fold repeat of the member is solved as a shooting system, with its half orbit (of duration t) cut into q pieces ($q = 8$ to 40, Online Resource 1, A.1). The unknowns are $Z = (u_1, u_2, t, \mathbf{s}_1, \ldots, \mathbf{s}_{q-1})$, with $\mathbf{s}_j$ the state at the start of the piece $j + 1$ and $\mathbf{s}_0$ the start (3) built from u_1, u_2 and λ, and the equations are

$$F_j = \Psi_{t/q}(\mathbf{s}_j) - \mathbf{s}_{j+1} \quad (j = 0, \ldots, q-2), \qquad F_{q-1} = \mathcal{R}\big(\Psi_{t/q}(\mathbf{s}_{q-1})\big) = 0, \tag{7}$$

where Ψ_τ is the flow over the time τ and $\mathcal{R}(\mathbf{x})$ has the three components of the departure of the state $\mathbf{x}$ from a collinear state with all velocities perpendicular to the line. For class I the start is (5) with the parameter η, and $\mathcal{R}$ has three components of the departure from an isosceles state (Online Resource 1, A.5). At a branch point the matrix $[J \,|\, \partial F/\partial\Lambda]$, with $J = \partial F/\partial Z$ and Λ the family parameter (λ in class C, η in class I), has a second null vector (the singular values for $n = 5$, 6 and 8 are in Online Resource 1, A.14). A second null vector is necessary for a second branch, and a quadratic bifurcation equation on the null space then has two real directions, the tangent of the repeat curve and the satellite (Online Resource 1, A.1 and A.19). That the second direction is real is a numerical result at each of the 52 members, not a consequence of the resonance. In this paper a crossing of a rotation number $1/n$ is a place on the trace of R where a rotation number passes $1/n$ (a bracket between two

stored points); the member found there is a candidate branch point (Section 2.2), it is a branch point when the matrix $[J \,|\, \partial F/\partial\Lambda]$ has a second null vector, shown by its singular values (computed for each of the 52 members of class C and the 16 of class I), and an end orbit is established when it meets the criterion of Section 3.3 (closure of the 30-digit orbit, an independent REBOUND integration and the syzygy sequence $(01)^n$).

The satellite curve is followed by pseudo-arclength continuation of the shooting system, in both directions from the branch point (called the senses $+1$ and -1) (the step rules are in Online Resource 1, A.1). The path length of a continuation is the Euclidean length of the curve in the space of the unknowns (Z, Λ), in the start units ($G = m = 1$, the outer bodies of the perpendicular start at distance 2 before the shift of the centre of mass). When θ changes sign between two accepted points, the zero of

$$\theta(Z, \Lambda) = 0 \tag{8}$$

is located by bisection along the chord, (Online Resource 1, A.1); a continuation ends at a zero of θ or at a limit of the method (Section 6). Each zero is tested for its syzygy sequence and for repeats (Online Resource 1, A.1); a syzygy is a collinear configuration, and the syzygy sequence is the cyclic list of the bodies in the middle at the successive syzygies. The same procedure, with the isosceles start and its symmetric residual, is used for class I.

The continuation of periodic orbits of conservative and Hamiltonian systems along their families has been developed in the literature (Muñoz Almaraz et al. 2003, 2007) and applied to the three-body problem (Doedel et al. 2003), among other things to the figure-eight orbit (Galán et al. 2002). The continuation used here is a pseudo-arclength continuation of a multiple-shooting system with boundary conditions fixed by the symmetry of the orbit; what is specific to this work is not a numerical method but its use, at the members of one family where a rotation number is $1/n$, followed to rotation angle 0 in two classes of symmetric orbits, with the end orbits refined and their multipliers computed in multiple precision. No claim is made that the numerical method differs from that of the cited papers.

2.4 Refinement and closure

Each zero is refined by Newton's method with a multiple-precision integrator (Gragg–Bulirsch–Stoer, in mpmath (), 40 digits), with the four unknowns of the start and the four end conditions of a zero of θ; the values are written with 30 digits. The closure is checked at three levels: in double precision with two integrators (the largest difference of a component after one period, best rotation removed, below 1×10^{-8} is called "reliable", orbits that do not meet this "weak"), with REBOUND (IAS15; Rein and Liu 2012; Rein and Spiegel 2015) from the start values rounded to double precision, and in 30 digits, integrating the full period from the values as stored (Online Resource 1, A.14). The numbers of this paper are those of the 30-digit orbits and do not depend on the double-precision zeros of the continuation (Online Resource 1, A.3).

2.5 Stability

The relative monodromy matrix of one relative period is $M = R(\theta) D\Psi_T(\mathbf{x}_0)$, the derivative of the flow over $T = 2t$ at the start state $\mathbf{x}_0$, followed by the rotation $R(\theta)$ of all positions and velocities by the angle θ of eq. (4). On the 8-dimensional part with zero centre of mass and momentum it has four trivial eigenvalues (associated with the time shift, the rotation and the two conserved quantities E and L), and the four others are the nontrivial multipliers. They are the eigenvalues of the 4×4 matrix N of the map induced by M on $W/\mathrm{span}\{\mathbf{f}, \mathbf{g}\}$,

$$W = \{\delta\mathbf{x} : \ \nabla E \cdot \delta\mathbf{x} = 0, \ \nabla L \cdot \delta\mathbf{x} = 0\}, \qquad N = \big[\, M \,\big]_{W/\mathrm{span}\{\mathbf{f},\mathbf{g}\}}, \tag{9}$$

with $\mathbf{f}$ the vector field of the equations of motion and $\mathbf{g}$ the generator of the rotation. The eigenvalues of N come in two pairs μ, $1/\mu$. The pair that makes the n-fold repeat degenerate at the branch point (the pair that is at $+1$ there) is the resonant pair, and the other is the transverse pair. At the end orbits the resonant pair was identified as the pair nearest $+1$. Along the curves it is followed by continuity from the first point at which it can be classified (Online Resource 1, A.13). The tracking by continuity is unambiguous, and at the zero of every curve the tracked pair is the pair nearest $+1$, so that the two identifications agree (Online Resource 1, A.13). In double precision the pair cannot be classified near the branch point itself (Section 3.3). A pair on the unit circle is written $\exp(\pm 2\pi i\alpha)$ with the angle α in turns (α_r and α_t), a real pair has the moduli μ_r, $1/\mu_r$ or μ_t, $1/\mu_t$, positive or negative. A pair on the unit circle, not at ± 1, is called elliptic, and a real pair, real positive or real negative, hyperbolic. An orbit is called spectrally stable when all nontrivial multipliers have modulus 1 to the numerical accuracy, and unstable otherwise; only the multipliers were computed, so nothing more than spectral stability is claimed, and the largest modulus is called the largest multiplier. For $n = 5$ to 12 the matrix is computed again in multiple precision, with the trivial multipliers removed by reduction and not by picking the four eigenvalues closest to 1; the class C orbits of $n = 13$ to 20 and the end orbits of class I ($n = 5$ to 20) are treated in the same way, with the 30-digit orbit only (details and error estimates in Online Resource 1, A.4 and A.14). The long-time behaviour of the stable orbits was tested with REBOUND (Section 3.2).

2.6 Rules written before the runs

The tolerances, predictions and time limits of each run were written into a rules file before the run (`docs/rules/`), and later changes were declared there before they were run. The failed predictions, the declared changes and the run times are listed in Online Resource 1 (A.12).

3 Results

3.1 The sequence of orbits in class C

Each member of R with the upper rotation number $\nu = 1/n$ starts a satellite curve. Followed to $\theta = 0$ in class C, the curve reaches a periodic orbit for every n from 5 to

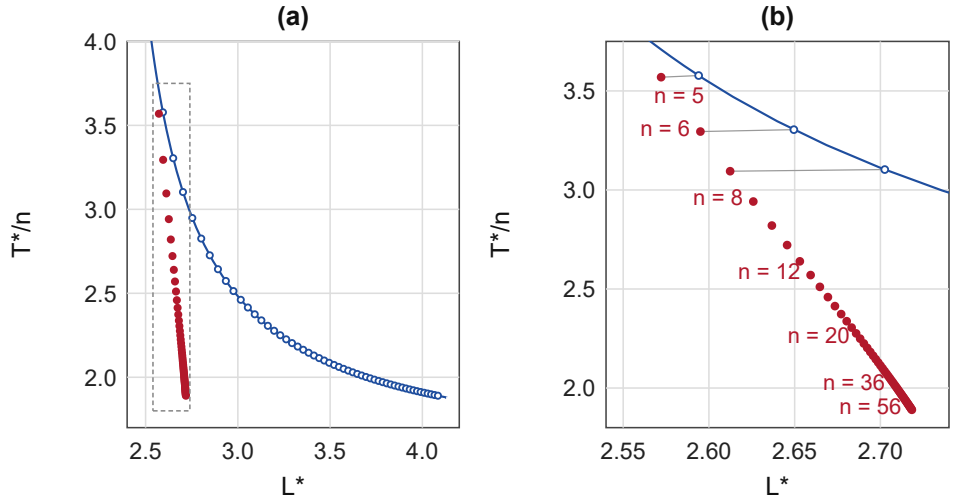


Fig. 2 (a) T^*/n against L^* for the family R (line), its members with $\nu = 1/n$ (open circles) and the end orbits of the satellite curves of class C (filled circles), $n = 5$ to 56. (b) Enlargement of the box drawn in (a), with some end orbits labelled by n; the grey lines join the member and the end orbit with the same n for the members inside the box.

56, which gives 52 orbits (Table 2). For $n = 5$ to 15 both senses of the curve reach $\theta = 0$ at the same orbit, started from its two symmetric points; from $n = 16$ on one sense reaches $\theta = 0$ and the other stops by a collapse of the step. The curves of $n = 5$ and 6 reach $\theta = 0$ a second time further on; these two orbits are not part of the sequence, and the continuation of the other curves stops at the first zero (Online Resource 1, A.1 and A.15). That the two end states are the two symmetric points of one orbit was checked on the double-precision end states of the continuation, with a largest difference of 1.9×10^{-9} in (u_1, u_2, λ) and 1.7×10^{-9} relative in t over $n = 5$ to 15 (Online Resource 1, A.15); the two senses are therefore linked by the flow over half a period (Section 2.1). Each of the 49 orbits for $n = 7$ and 9 to 56 has the syzygy sequence $(01)^n$, that is $2n$ syzygies, and no repeat in the return test, and so have the orbits for $n = 5$, 6 and 8 (Online Resource 1, A.8). One relative period of R is a single loop on the shape sphere, with the syzygy sequence (01), and a satellite in the sense of Janković et al. (2020) is an orbit whose topology is the k-th power of that of its progenitor; the orbits of the sequence are therefore satellites of R with the topological exponent $k = n$.

The orbits are stored with 30 digits and close over the full period to between 1.1×10^{-26} and 7.1×10^{-23} (Online Resource 1, A.8). T^* grows from 17.84681 at $n = 5$ to 105.84583 at $n = 56$, and T^*/n falls from 3.5694 to 1.8901; L^* grows from 2.57212 to 2.71835. The end orbit has a lower T^*/n and a lower L^* than the member of R with $\nu = 1/n$ (Fig. 2; the amounts are in Online Resource 1, A.8). This fits Hénon's relation (Section 4.1; the amounts are in Online Resource 1, A.15).

3.2 Stability of the end orbits of class C

The multipliers are given as the resonant and the transverse pair (Section 2.5; the resonant pair is the pair nearest $+1$). For $n = 5$ to 12 the end orbits are spectrally stable: in multiple precision, the four nontrivial multipliers are $\exp(\pm 2\pi i\alpha_r)$ and $\exp(\pm 2\pi i\alpha_t)$ with moduli equal to 1 within 3.6×10^{-24} for the 30-digit orbits and within 2.6×10^{-35} for the orbits refined to 40 digits. The resonant pair is at the angle α_r between 0.0039 ($n = 5$) and 0.0095 ($n = 7$ and 8) from $+1$, and the transverse pair at $\alpha_t = 0.1029$ at $n = 5$, rising to 0.4017 at $n = 12$ with growing steps (Table 2; Online Resource 1, A.8). The two angles of an orbit are distinct (the smallest difference is 0.099, at $n = 5$, Online Resource 1, A.8), so the 4×4 matrix N is diagonalisable and these orbits are also linearly stable in the reduced space; this is not a statement about the trivial multipliers. This is spectral stability at the accuracy of the computation, with error estimates from two precisions, not a proof. In double precision, REBOUND runs of 10,000 periods keep the orbits within 1.1×10^{-8} of the start state, and a perturbation grows linearly in the number of periods, the signature of a frequency shift and not of an instability (Online Resource 1, A.15).

From $n = 13$ on the end orbits are unstable. In multiple precision (the 30-digit orbit only) the transverse pair is real and negative (angle 0.5), with the moduli of Table 2 for $n = 13$ to 20, while the resonant pair is still on the unit circle, with modulus 1 within 7×10^{-25} and an angle between 0.0071 and 0.0082, inside the range of α_r for $n \le 12$. The largest multiplier (Table 2) is real and negative for every $n = 13$ to 56 (for $n = 21$ to 56 computed in double precision from the 30-digit orbit; Online Resource 1, A.13).

How the stability of the end orbits is lost can be read from the spectra of $n = 5$ to 20 and from the curves. In the spectra of the end orbits the angle α_t of the transverse pair rises towards $1/2$ and has reached it between the end orbits of $n = 12$ and $n = 13$: between these two end orbits the transverse pair is past -1, on the negative real axis. These end orbits are not on one family, so this implies neither a passage through -1 nor a bifurcation. Along each curve (Online Resource 1, A.13) the transverse pair is on the unit circle from the branch point to the end orbit for $n = 5$ to 12, in both classes, and for $n = 13$ to 20 it changes once from elliptic to real negative, before the end orbit, on every curve of both classes. This is a passage through -1, the case in which a period-doubling bifurcation is generically expected; whether one occurs on these curves was not examined. It is not a collision at $+1$ and not a collision of the two pairs. The passage lies above the end orbit in L^* for every $n = 13$ to 20 in both classes, and its L^* rises with n faster than that of the end orbit (the brackets are in Table S2 and the numbers in Online Resource 1, A.13). No complex quadruplet occurs. That the end orbits lose stability at $n = 13$ is therefore a statement about where the end orbit lies relative to this passage: for $n \ge 13$ it lies beyond the passage, and for $n \le 12$ no passage through -1 is seen between the branch point and the end orbit (one point past the end orbit of the class I curve of $n = 12$, sense -1, is already real negative; it is a single point and is not counted). This is a reading of what was computed: n is a label and not a parameter, no single family was followed through the value of n at which the passage would meet the end orbit, and why the passage lies where it does was not examined.

Table 2: The periodic orbits on the satellite curves of the family R in class C, upper rotation number $\nu = 1/n$, $n = 5$ to 56. T^* and L^* are the scale-free period and angular momentum of one relative period. For $n = 5$ to 12 the angles α_r and α_t (in turns) of the resonant and of the transverse pair, all four multipliers having modulus 1; for $n \geq 13$ the modulus of the largest multiplier (real and negative for every $n \geq 13$; for $n = 13$ to 20 it is the transverse pair, and for $n \geq 21$ the pair it belongs to was not examined). The last column gives the number of senses of the continuation that reach $\theta = 0$.

n	T^*	L^*	α_r	α_t	largest multiplier (modulus)	senses with $\theta = 0$
5	17.84681	2.57212	0.003945	0.102903	1 (stable)	2 of 2
6	19.76913	2.59503	0.008370	0.121714	1 (stable)	2 of 2
7	21.66265	2.61237	0.009486	0.156989	1 (stable)	2 of 2
8	23.53271	2.62588	0.009528	0.196283	1 (stable)	2 of 2
9	25.38320	2.63672	0.009294	0.237628	1 (stable)	2 of 2
10	27.21709	2.64560	0.008999	0.282125	1 (stable)	2 of 2
11	29.03666	2.65302	0.008709	0.333142	1 (stable)	2 of 2
12	30.84374	2.65930	0.008442	0.401722	1 (stable)	2 of 2
13	32.63981	2.66470	–	–	1.712	2 of 2
14	34.42608	2.66938	–	–	2.609	2 of 2
15	36.20357	2.67349	–	–	3.426	2 of 2
16	37.97312	2.67712	–	–	4.235	1 of 2
17	39.73547	2.68034	–	–	5.054	1 of 2
18	41.49124	2.68323	–	–	5.890	1 of 2
19	43.24098	2.68584	–	–	6.745	1 of 2
20	44.98515	2.68820	–	–	7.621	1 of 2
21	46.72419	2.69035	–	–	8.519	1 of 2
22	48.45845	2.69231	–	–	9.439	1 of 2
23	50.18826	2.69411	–	–	10.381	1 of 2
24	51.91392	2.69577	–	–	11.346	1 of 2
25	53.63569	2.69730	–	–	12.333	1 of 2
26	55.35381	2.69872	–	–	13.342	1 of 2
27	57.06850	2.70004	–	–	14.374	1 of 2
28	58.77994	2.70127	–	–	15.427	1 of 2
29	60.48832	2.70242	–	–	16.502	1 of 2
30	62.19380	2.70349	–	–	17.599	1 of 2
31	63.89653	2.70450	–	–	18.717	1 of 2
32	65.59664	2.70545	–	–	19.857	1 of 2
33	67.29427	2.70635	–	–	21.018	1 of 2
34	68.98953	2.70719	–	–	22.199	1 of 2
35	70.68253	2.70799	–	–	23.402	1 of 2
36	72.37337	2.70874	–	–	24.624	1 of 2
37	74.06214	2.70946	–	–	25.868	1 of 2
38	75.74893	2.71014	–	–	27.131	1 of 2
39	77.43383	2.71078	–	–	28.415	1 of 2
40	79.11690	2.71140	–	–	29.719	1 of 2
41	80.79823	2.71199	–	–	31.042	1 of 2
42	82.47787	2.71254	–	–	32.385	1 of 2
43	84.15589	2.71308	–	–	33.748	1 of 2
44	85.83236	2.71359	–	–	35.130	1 of 2
45	87.50731	2.71408	–	–	36.531	1 of 2
46	89.18082	2.71455	–	–	37.951	1 of 2
47	90.85292	2.71500	–	–	39.391	1 of 2
48	92.52367	2.71543	–	–	40.849	1 of 2
49	94.19311	2.71585	–	–	42.325	1 of 2
50	95.86129	2.71625	–	–	43.821	1 of 2
51	97.52823	2.71663	–	–	45.334	1 of 2
52	99.19399	2.71700	–	–	46.867	1 of 2
53	100.85859	2.71736	–	–	48.417	1 of 2
54	102.52208	2.71770	–	–	49.985	1 of 2
55	104.18448	2.71803	–	–	51.572	1 of 2
56	105.84583	2.71835	–	–	53.176	1 of 2

3.3 A second family for $n = 5$ to 20

The second reversing symmetry of R defines class I (Section 2.1). For every $n = 5$ to 20 the member with $\nu = 1/n$ is found in the isosceles description and the n-fold repeat closes with 8 pieces, with the same two-dimensional null space of the shooting matrix as in class C and two real roots of the bifurcation equation, the direction of the repeat and one other (Online Resource 1, A.9). The curve of the non-repeat root reaches $\theta = 0$ in both senses for $n = 5$ to 14 and in one sense for $n = 15$ to 20, the other sense stopping by a collapse of the step; where both senses reach $\theta = 0$ they reach the same orbit, started from its two symmetric points. For $n = 14$ the zero of sense -1 is less converged, on the same curve (Online Resource 1, A.15). Both curves leave the branch point on the same side as the satellites of class C, with L^* below the branch value: L^* minus that of the member is never above zero along the curves (Online Resource 1, A.9).

For every $n = 5$ to 12 the computation gives, from the same branch point and on the same side, a stable orbit of class C and an unstable orbit of class I. The two end orbits are close and not equal. T^* and L^* of the class I orbit differ from those of the class C orbit by amounts far above the closures (Table 3). The class C orbit has all four nontrivial multipliers on the unit circle. In the class I orbit the resonant pair is real positive, μ_r between 1.025 and 1.062 (and its inverse), and the transverse pair is on the unit circle, at an angle α_t that is above that of the class C orbit by 0.0004 at $n = 5$ and by 0.0489 at $n = 12$ (Online Resource 1, A.9). The results show no difference between odd and even n.

For $n = 13$ to 20 both end orbits are unstable. In both classes the transverse pair has left the unit circle on the negative real axis (the moduli are in Tables 4 and 5). In class I the angle α_t of the transverse pair has reached $1/2$ between $n = 12$ and $n = 13$, as it did in class C (Table 5). The resonant pair is elliptic in class C, with a small angle, and real positive in class I (Table 5). The largest multiplier of the class I orbit is above that of the class C orbit, by 26 percent at $n = 13$ and 11 percent at $n = 20$. The differences in T^* and L^* are in Table 4. The end orbit of class I is lower in L^* than the member of R by 0.313 at $n = 13$ and 0.544 at $n = 20$.

Each end orbit of class I is established by a criterion (fixed before the runs for $n = 6$ to 20, added after the data for $n = 5$): the closure of the 30-digit orbit, an independent integration with REBOUND (IAS15) that closes the start values after one period, and the syzygy sequence $(01)^n$ (the limits are in Online Resource 1, A.9). The same three tests were made for the class C orbits, with limits that were not fixed in advance. The closure of the 30-digit orbits is 1.1×10^{-26} to 7.1×10^{-23} and the syzygy sequence is $(01)^n$ for all 52. REBOUND, from the 30-digit start rounded to double precision, closes the 49 orbits for $n = 7$ and 9 to 56 to 1.6×10^{-14} to 1.5×10^{-12}; for $n = 5$, 6 and 8 a different REBOUND check was made, from the double-precision starts of the continuation and not from the 30-digit starts, with closures 2.3×10^{-11}, 8.5×10^{-11} and 2.6×10^{-10} (for $n = 8$ over the double-length orbit).

The four nontrivial multipliers were also computed at every point of the 53 curves that reach $\theta = 0$ (both classes, $n = 5$ to 20), in double precision by the reduction of Section 2.5, and the types of the two pairs were followed by continuity (Online Resource 1, A.13 and Table S2). Near the branch point the resonant pair lies within

the noise of the double multiplier +1 and cannot be classified in double precision; it is classified only from a path length of 0.76 to 4.9 on (for $n = 5$ at $L^* = 2.5865$, Online Resource 1, A.13), so nothing is said about its type at the branch point. For $n = 5$ the resonant pair is elliptic in class C and real positive in class I over the classified part, as at the end orbits, and no change was seen from the first classified point to the end. For $n = 6$ to 20, over the part of each curve where the type can be read, the type of the resonant pair is opposite to its type at the end orbit, and it changes once on each of these 49 curves: in class C the resonant pair is real positive from the first classified point and becomes elliptic before the end orbit, and in class I it is elliptic and becomes real positive. The type near the branch point could not be determined. The change takes place at nearly the same L^* in the two classes (all brackets are in Table S2; the numbers for $n = 12$ and the distances of the centres of the brackets are in Online Resource 1, A.13). The change lies at 0.42 ($n = 6$) to 0.90 ($n = 20$) of the way from the branch point to the end orbit, measured in L^* (the definition of this fraction is in Online Resource 1, A.13). At the end orbits the resonant pair is therefore elliptic in class C and real positive in class I, as in Table 5, and along the curves, for $n \geq 6$, it is not (what is open is stated in Section 6.2). The transverse pair is described in Section 3.2.

At the branch point the two families are not separated by their invariants. For $n = 5$ the two curves agree in (T^*, L^*, θ) to 1×10^{-9} over the first 0.23 of the path length, and then separate: at equal L^*, T^* of the class I curve exceeds that of the class C curve by up to 2.0×10^{-4} near the end (Fig. 3). That the end orbit of class I is a different orbit from the class C orbit of the same n rests on three facts. Its symmetry is different: it has an isosceles state, fixed by S', and no state fixed by S, the reverse of the class C orbit. Its multiplier structure is different: at the end orbit its resonant pair is real positive for every $n = 5$ to 20 (1.0252 and 0.9754 at $n = 5$), where that of the class C end orbit is on the unit circle. And the differences of Table 3 and Table 4, in T^* and L^*, are many orders above the closures of the orbits (4×10^{-26} to 4×10^{-24}; for $n = 5$, 3.0×10^{-7} and 6.2×10^{-5} against the closure of the same orbit in Table 3). For $n = 5$ the comparison of the two curves written down before the run was undecided, and these three facts were added after the data were seen; for $n = 6$ to 20 the criterion was written before the runs (Online Resource 1, A.5 and A.12).

The two pairs of the end orbits of both classes are listed in Table 5. The elliptic–hyperbolic split of the resonant pair therefore holds at the end orbits for every $n = 5$ to 20 (along the curves it does not hold for $n \geq 6$, Section 3.3); what changes at $n = 13$ is the transverse pair, in both classes.

Interpretation. The split of the resonant pair at the end orbits into an elliptic pair (class C) and a hyperbolic pair (class I), for every $n = 5$ to 20, is qualitatively analogous to the pair of orbits of period k that appear in a generic period-k bifurcation of a two-dimensional area-preserving map for $k \geq 5$: on one side of the critical value only, two orbits of period k appear, one elliptic and one hyperbolic, both approaching the fixed point (Meyer 1970, Proposition 1.18). Meyer's theorem concerns the neighbourhood of the branch point, where the types could not be resolved; the analogy is therefore made for the end orbits and not for the curves, along which the type of the resonant pair, where it can be read, is opposite to that at the end orbit and changes

Table 3 The periodic orbits at the end of the class I curves, upper rotation number $\nu = 1/n$. The fourth and fifth columns give T^* and L^* of the class I orbit minus those of the class C orbit of the same n, absolute with the relative value in brackets; the sixth gives the real pair of multipliers (the resonant pair; the product is 1); the seventh the angle α_t (in turns) of the transverse pair, whose modulus is 1 within 4.1×10^{-25}. All eight orbits have an isosceles state and no state fixed by S. All values are from the 30-digit orbits. Table 4 gives $n = 13$ to 20.

n	T^*	L^*	$T^*(I) - T^*(C)$	$L^*(I) - L^*(C)$	resonant pair μ_r, $1/\mu_r$	transverse pair α_t	closure (30 digits)
5	17.84680795	2.57205342	3.02×10^{-7} (1.69×10^{-8})	-6.25×10^{-5} (-2.43×10^{-5})	1.025201 / 0.975419	0.103322	4.4×10^{-26}
6	19.76913346	2.59476079	1.93×10^{-6} (9.75×10^{-8})	-2.74×10^{-4} (-1.06×10^{-4})	1.053890 / 0.948866	0.124194	6.0×10^{-26}
7	21.66265442	2.61183107	3.99×10^{-6} (1.84×10^{-7})	-5.35×10^{-4} (-2.05×10^{-4})	1.061202 / 0.942328	0.161694	2.6×10^{-25}
8	23.53271307	2.62507903	5.92×10^{-6} (2.52×10^{-7})	-8.02×10^{-4} (-3.05×10^{-4})	1.061555 / 0.942014	0.203392	1.2×10^{-25}
9	25.38321068	2.63565692	7.57×10^{-6} (2.98×10^{-7})	-1.06×10^{-3} (-4.02×10^{-4})	1.060091 / 0.943315	0.247655	5.7×10^{-26}
10	27.21709891	2.64429888	8.95×10^{-6} (3.29×10^{-7})	-1.30×10^{-3} (-4.91×10^{-4})	1.058227 / 0.944977	0.296197	2.9×10^{-25}
11	29.03667260	2.65149243	1.01×10^{-5} (3.47×10^{-7})	-1.52×10^{-3} (-5.74×10^{-4})	1.056381 / 0.946628	0.354303	2.3×10^{-25}
12	30.84375584	2.65757385	1.10×10^{-5} (3.58×10^{-7})	-1.73×10^{-3} (-6.50×10^{-4})	1.054674 / 0.948160	0.450630	3.7×10^{-25}

Table 4 The periodic orbits at the end of the class I curves for $n = 13$ to 20. Columns 2 to 5 as in Table 3. Both orbits are unstable: columns 6 and 7 give the resonant pair (real positive) and the transverse pair (real negative) of multipliers of the class I orbit $(\mu, 1/\mu)$, column 8 the transverse pair (real negative) of the class C orbit (multiple precision, the 30-digit orbit only); the class I orbit has no pair on the unit circle, the class C orbit its resonant pair on it, with a small angle. All eight orbits have an isosceles state and no state fixed by S. All values are from the 30-digit orbits.

n	T^*	L^*	$T^*(I) - T^*(C)$	$L^*(I) - L^*(C)$	class I: resonant pair μ_r, $1/\mu_r$	class I: transverse pair μ_t, $1/\mu_t$	class C: transverse pair μ_t, $1/\mu_t$	closure (30 digits)
13	32.63982557	2.66278267	1.18×10^{-5} (3.62×10^{-7})	-1.92×10^{-3} (-7.19×10^{-4})	1.053132 / 0.949549	-2.163849 / -0.462139	-1.712033 / -0.584101	6.8×10^{-25}
14	34.42609651	2.66729419	1.25×10^{-5} (3.63×10^{-7})	-2.09×10^{-3} (-7.83×10^{-4})	1.051749 / 0.950797	-3.053446 / -0.327499	-2.609028 / -0.383285	5.7×10^{-25}
15	36.20358137	2.67123965	1.30×10^{-5} (3.60×10^{-7})	-2.25×10^{-3} (-8.41×10^{-4})	1.050510 / 0.951918	-3.912176 / -0.255612	-3.425850 / -0.291898	3.5×10^{-24}
16	37.97313436	2.67471932	1.35×10^{-5} (3.56×10^{-7})	-2.40×10^{-3} (-8.95×10^{-4})	1.049398 / 0.952928	-4.775913 / -0.209384	-4.235237 / -0.236114	1.4×10^{-24}
17	39.73548355	2.67781109	1.39×10^{-5} (3.50×10^{-7})	-2.53×10^{-3} (-9.45×10^{-4})	1.048395 / 0.953839	-5.655690 / -0.176813	-5.054411 / -0.197847	2.1×10^{-24}
18	41.49125514	2.68057642	1.43×10^{-5} (3.44×10^{-7})	-2.66×10^{-3} (-9.91×10^{-4})	1.047489 / 0.954664	-6.556083 / -0.152530	-5.889980 / -0.169780	1.8×10^{-24}
19	43.24099217	2.68306444	1.46×10^{-5} (3.37×10^{-7})	-2.78×10^{-3} (-1.03×10^{-3})	1.046665 / 0.955415	-7.479251 / -0.133703	-6.744992 / -0.148258	3.6×10^{-24}
20	44.98516898	2.68531489	1.49×10^{-5} (3.30×10^{-7})	-2.88×10^{-3} (-1.07×10^{-3})	1.045914 / 0.956102	-8.426266 / -0.118677	-7.620986 / -0.131217	2.1×10^{-24}

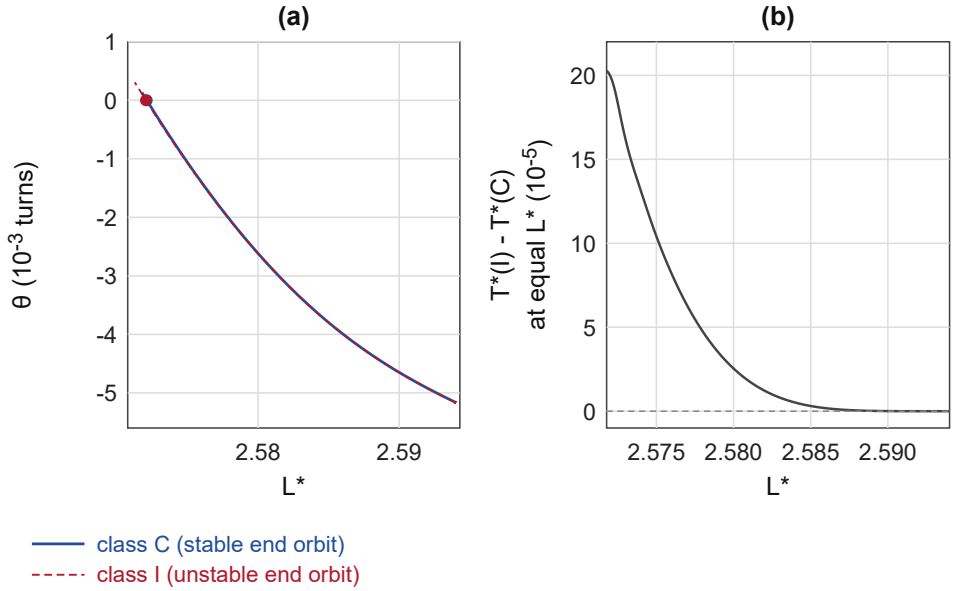


Fig. 3 The two satellite families for $n = 5$. (a) The rotation angle of the full period against L^* along the curve of class C (full line) and of class I (dashed); the two end orbits ($\theta = 0$) are marked (they coincide at this scale). (b) T^* of the class I curve minus T^* of the class C curve at equal L^*, from the splines of the two stored curves.

once (Section 3.3). The theorem is for maps of a two-dimensional manifold without symmetry; the reduced map here is four dimensional and reversible, so the theorem does not apply directly, and the split is a numerical result of this computation, not a consequence of the theorem. For involutory (reversible) area-preserving maps, which arise from Hamiltonian systems with two degrees of freedom and a symmetry, Rimmer (1980) states that the generic bifurcations at roots of unity other than ± 1 have the form of Meyer's, with every bifurcating periodic point symmetric. His results are for maps of the plane, and the reduced map here is four-dimensional, so this is an analogy only, as with Meyer. The general theory of subharmonic bifurcation in time-reversible systems is developed by Vanderbauwhede (1986); a detailed comparison with the present results is not attempted here. The pairing of a stable and an unstable end orbit exists for $n = 5$ to 12 only: from $n = 13$ the transverse pair is real negative in both classes (Table 5), and both orbits are unstable.

3.4 The family R beyond the end of the stored trace

The stored trace of R stops at $L^* = 4.129$ ($T^* = 1.880$) with $\nu_{\mathrm{lo}} = 0.017034$ and $\nu_{\mathrm{up}} = 0.017100$, both still falling. The end of the stored trace is a limit of the tool (a step rule on the half period) and not a property of the family (Online Resource 1, A.15). The trace was continued from the last stored point with the same code, in two runs, to $L^* = 7.25$ ($\lambda = 0.970$, $T^* = 1.646$): 109 stored points, of which 78 are distinct

Table 5 The resonant and the transverse pair of nontrivial multipliers of the end orbits of the two classes, $n = 5$ to 20 (multiple precision, the 30-digit orbits). The resonant pair is the pair nearest $+1$. Angles α in turns, with the distance $1/2 - \alpha$ from -1 in brackets; for a real pair the modulus μ, the other multiplier being $1/\mu$.

n	class C: resonant pair, α_r	class C: transverse pair	class I: resonant pair, μ_r	class I: transverse pair
5	0.0039	$\alpha_t = 0.1029$ (0.397)	1.0252	$\alpha_t = 0.1033$ (0.397)
6	0.0084	$\alpha_t = 0.1217$ (0.378)	1.0539	$\alpha_t = 0.1242$ (0.376)
7	0.0095	$\alpha_t = 0.1570$ (0.343)	1.0612	$\alpha_t = 0.1617$ (0.338)
8	0.0095	$\alpha_t = 0.1963$ (0.304)	1.0616	$\alpha_t = 0.2034$ (0.297)
9	0.0093	$\alpha_t = 0.2376$ (0.262)	1.0601	$\alpha_t = 0.2477$ (0.252)
10	0.0090	$\alpha_t = 0.2821$ (0.218)	1.0582	$\alpha_t = 0.2962$ (0.204)
11	0.0087	$\alpha_t = 0.3331$ (0.167)	1.0564	$\alpha_t = 0.3543$ (0.146)
12	0.0084	$\alpha_t = 0.4017$ (0.098)	1.0547	$\alpha_t = 0.4506$ (0.049)
13	0.0082	real negative, $\mu_t = 1.712$	1.0531	real negative, $\mu_t = 2.164$
14	0.0080	real negative, $\mu_t = 2.609$	1.0517	real negative, $\mu_t = 3.053$
15	0.0078	real negative, $\mu_t = 3.426$	1.0505	real negative, $\mu_t = 3.912$
16	0.0076	real negative, $\mu_t = 4.235$	1.0494	real negative, $\mu_t = 4.776$
17	0.0075	real negative, $\mu_t = 5.054$	1.0484	real negative, $\mu_t = 5.656$
18	0.0073	real negative, $\mu_t = 5.890$	1.0475	real negative, $\mu_t = 6.556$
19	0.0072	real negative, $\mu_t = 6.745$	1.0467	real negative, $\mu_t = 7.479$
20	0.0071	real negative, $\mu_t = 7.621$	1.0459	real negative, $\mu_t = 8.426$

to 5 decimals in (λ, L^*) (the two runs and the join are described in Online Resource 1, A.19). All the points are stable, and with the stored trace the rotation numbers $1/n$ are crossed for every n from 3 to 439 (details in Online Resource 1, A.19). These crossings are brackets and not computed branch points: no satellite was computed beyond $n = 56$, the family was not followed beyond the end of the extended trace, and no claim is made that the sequence of satellites ends. The files are listed in Online Resource 1, A.11.

4 The period of the orbits and the angular momentum

4.1 Hénon's relation along a satellite curve

The satellite curve leaves the n-fold repeat of a member of R, so the T^* of its end orbit is close to nT^*_{member}. Write $\delta_n = nT^*_{\text{member}} - T^*(\text{end orbit})$, with the exact member. Hénon (1977) shows, for a family of periodic solutions with an axis of symmetry, that $\partial T/\partial A = -\partial\Phi/\partial E$ (his eq. 30), with T the period, A the angular momentum, Φ the rotation angle after one period and E the energy, and, for the N-body problem, with the similarity of Newtonian orbits, that $dT/d\Phi = -A/(2E)$ along a family of fixed energy (his eq. 35); the steps to scale-free variables are in Online Resource 1, A.16. Since $\theta = -\Phi$, with $T^* = T|E|^{3/2}$ and $L^* = |A||E|^{1/2}$ the relation reads

$$dT^* = -\frac{L^*}{2}\, d\theta = -\pi L^*\, d\rho, \tag{10}$$

with $\rho = \theta/2\pi$ the rotation in turns. The sign and the size of dT^* were checked on the stored curves (Online Resource 1, A.10). He states that it had been verified numerically for the plane three-body problem (Hénon 1976).

Along a satellite curve the relation gives $\delta_n = \pi \int L^* d\rho$, with ρ from $-\varepsilon_n$ to 0 turns, where $\varepsilon_n = n|\rho_R| - 1$ is the excess of the n-fold repeat of the member (ρ_R its rotation in turns) over a whole number of turns; the integral is positive. For all 52 curves the integral, computed with the trapezoid rule on the stored points, equals δ_n with a ratio of 1.0000 and a largest difference of 4.1×10^{-7} in T^*. This is a numerical verification of Hénon's relation on the satellite curves and a check of the stored numbers, not a result of this paper. The slope check at the branch point is in Online Resource 1, A.16.

4.2 What predicts δ_n

Three predictions of the T^* of the end orbit were compared: no correction, the first-order prediction from eq. (10), and an empirical relation B, written down before the runs for $n \geq 21$, with two constants fitted on $n = 8$ to 20. The first-order prediction is the best of the three for $n \leq 12$ (error 0.0037 at most); the bounds written before the runs do not separate B from no correction (Online Resource 1, A.7 and A.19). B is kept as an empirical remark and not as a result. The definitions, Table S1 and the statistics are in Online Resource 1, A.7.

4.3 The dip of the rotation: an open question

Along the satellite curve θ does not go straight from $-\varepsilon_n$ to 0: it first becomes more negative and then rises to 0 (Fig. 4). The depth of the dip below $-\varepsilon_n$ is 0 for $n = 5$ and 6, 1.4×10^{-4} turns for $n = 9$, 1.1×10^{-3} for $n = 15$, 1.7×10^{-3} for $n = 25$, 2.0×10^{-3} for $n = 36$ and 2.1×10^{-3} for $n = 56$; it equals ε_n at $n = 26$ and is larger than ε_n from $n = 27$. The lowest θ of the dip is the highest T^*, a coincidence of extrema that the relation of Hénon implies, on 51 of the 52 curves at the same stored point and on the 52nd at neighbouring points (Online Resource 1, A.15). With $\delta_n = \pi \int L^* d\rho$, the integral has two legs of opposite sign: on the way down L^* is high, on the way up it is lower, and the legs nearly cancel, which is why the mean slope δ_n/ε_n is below πL^* of the end orbit for large n (6.13 against 8.51 at $n = 36$) and why the slope at the branch point cannot give δ_n beyond n of about 12. The size of the dip, and the curve of L^* against θ that goes with it, decide δ_n; they are not predicted by the R family alone, and the dip is not explained here.

5 Comparison with the literature

5.1 Davoust and Broucke (1982)

Their family D1 is Broucke's R: the rows $N = 62$ to 67 of their Table 5 lie on the curve of R traced here. On D1 they find three bifurcations: the branch e (triple period), f (double period) and E (triple period). The satellites computed here from the members with $\nu = 1/3$ pass through the rows 79 to 81 of the branch e and the rows 71 to 78 of the branch E, to 3×10^{-6} or better in T^* and L^* and with the same rotation angle; the branch f ($n = 2$) was not followed here. The satellites of R

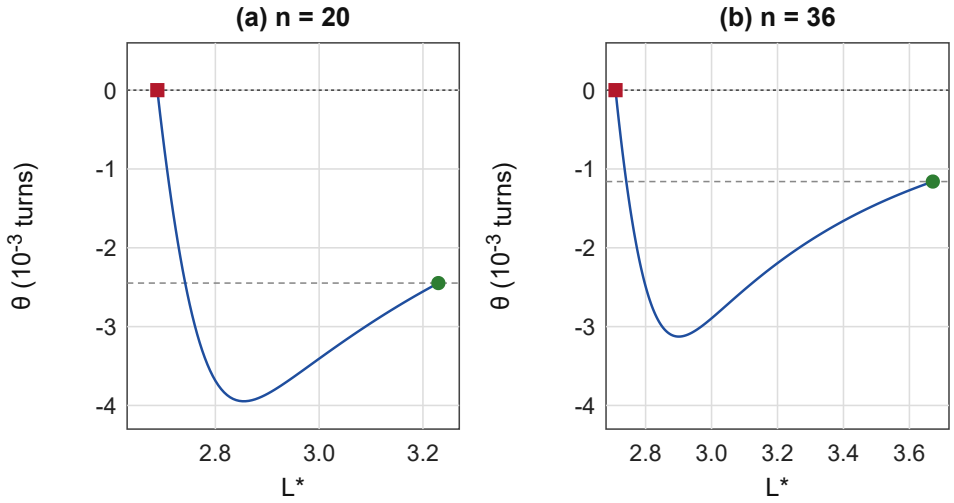


Fig. 4 The rotation angle of the full period along the satellite curve, from the branch point (green circle) to the end orbit (red square), against L^*, for (a) $n = 20$ and (b) $n = 36$. The dashed line is the rotation $-\varepsilon$ of the n-fold repeat at the branch point. For $n = 20$: $-\varepsilon = -2.448 \times 10^{-3}$ turns, the lowest point of the curve is -3.947×10^{-3} turns, 1.499×10^{-3} below $-\varepsilon$. For $n = 36$: $-\varepsilon = -1.160 \times 10^{-3}$ turns, the lowest point is -3.127×10^{-3} turns, 1.967×10^{-3} below $-\varepsilon$.

for $n = 2$ and 3 were therefore published in 1982; for $n \geq 4$ that paper has nothing, since its authors stopped at the multiplicity three. The rows 90 and 91 of their table, called "the first ($k = 3$) satellite" of the BHH family by Janković and Dmitrašinović (2016) and Janković et al. (2020), are a different pair: they counter-rotate, so they are retrograde (T^* 9.67 and 9.66, L^* 1.05 and 1.04).

5.2 The Three Body Orbits atlas

The atlas () has satellites of the BHH family coded by branch (R prograde, A retrograde), 14 of them with equal masses, from its own search of September 2026 and with no paper cited. Its entry R7 1/1 agrees with the class C orbit for $n = 7$: T^* to 1×10^{-12} and L^* to 1.6×10^{-6}, the digits of the entry. No other class C orbit of the sequence was found in the atlas. The comparison used the local copy of 2026-10-09 of all 415 equal-mass entries with non-zero angular momentum (the catalogue was not downloaded again), with the matching criteria of Online Resource 1, A.17. The 16 class I end orbits ($n = 5$ to 20) were compared in the same way with the 415 entries and with the 99 satellites of the CPC tables: none matches at 1×10^{-5}, and the only entries within 5×10^{-3} are the atlas entry R7 1/1 for $n = 7$, which is the class C orbit, and, for $n = 17$, two CPC rows at twice T^*, which is a coincidence of two numbers (details in Online Resource 1, A.17). The atlas has no versioned DOI and cites no paper, so the comparison is weak evidence either way. The checksum of the local copy of the catalogue is in `docs/results.md` of the repository.

5.3 The preliminary orbits of Janković

Janković et al. (2020, Section 4, p. 8) report the two preliminary searches of Section 1.4, with six satellites, $k = 84$, 12, 45, 39, 58 and 13, "some of which are retrograde and others are direct". The six orbits are in the master thesis of M. R. Janković (MSc thesis, University of Belgrade, 2016; copy provided by the author; appendix A), which is not publicly available. The orbits were converted like the rows of the CPC tables, closed again and tested, with the following result. The orbit $k = 39$ is a rotating member (θ not 0) of the satellite curve of the member of R with the lower $\nu = 1/39$; the orbit with $\theta = 0$ on this curve was not computed (further details in Online Resource 1, A.17). The orbit $k = 45$ is a 45-fold repeat of an orbit of R, and not a satellite. The orbits $k = 58$, 12 and 84 are undecided; for $k = 58$, whose refined version is the row $N = 99$ of the CPC tables, the family could not be followed from its start. So at most two of the six orbits, $k = 39$ and perhaps $k = 58$, are points of satellite curves of R, and $k = 45$ is a repeat. No value of the thesis is quoted in this paper, and none is needed for this statement.

5.4 The 99 satellites of the CPC tables, and the work of Li and Liao

None of the 99 rows of the CPC tables, relatively periodic orbits with θ not 0, lies on a satellite curve of R computed here: 95 are excluded by a screen on T^*/k; $N = 9$ lies on the branch with $k = 5$ of the BHH orbit A1; $N = 19$ and 33 are near the traced curve of Hénon's family; $N = 99$ ($k = 58, L^* = 3.26$) is open. Li and Liao (2020, arXiv:2008.13550) computed 598,996 orbits of the BHH family and its satellites with unequal masses, all retrograde; Liao et al. (2022) continue equal-mass base orbits to unequal masses; neither treats the prograde branch. Li et al. (2025) continue the figure-eight and IA-3 orbits from zero angular momentum and give 18 rows, 16 of them with $L^* > 0$ (the other two are the orbits with zero angular momentum). None of the 68 orbits of this paper (the 52 of class C and the 16 of class I of the supplement) is within 5×10^{-3} in T^* and L^* of one of the 16 rows with $L^* > 0$, with repeats up to 12 allowed on either side; the rows have L^* below 0.36 and the orbits above 2.57, so the comparison is decided by L^* alone.

5.5 What was not found

In the sources checked, no work was found that lists, computes or describes the orbits with $\theta = 0$ on the satellite curves of R at $\nu = 1/n$ with $n \geq 5$, or their sequence, other than Davoust and Broucke ($n = 2$ and 3) and the atlas entry for $n = 7$; and none was found that describes a second family of satellites at these branch points. The sources checked are described in Section 6.3.

6 Limitations

The results are computational: the bifurcation results for area-preserving maps quoted in Section 1.5 do not cover the four-dimensional reduced map, and nothing in this paper is derived from them.

6.1 What was not searched or decided

The second family (class I) was computed for the upper rotation number and $n = 5$ to 20 only: it was searched for $n = 13$ to 20, where the satellites of class C are already unstable, and not for $n \geq 21$, nor for the lower rotation number, and orbits without these symmetries were not searched. For $n = 5$ to 20 the null space of the shooting matrix is two dimensional in both classes, so there is no further root of the bifurcation equation in them. Whether other families of satellites exist at the branch points is not decided. The types of the multipliers along the curves were determined for the 53 curves of $n = 5$ to 20 that reach $\theta = 0$, in the two classes and up to the first zero; for $n = 21$ to 56 only the sign and the modulus of the largest multiplier of the end orbit were computed, and the curves that stop at a limit, the lower rotation number and the part beyond the zero were not examined.

The upper branch for $n = 4$ was not decided. The cases $n = 57$ and 58 are undecided: both senses of both curves stopped at the step limit (Online Resource 1, A.19); a further change of the method for these two cases was declared before it was run, and its results are not part of this paper. The sequence ends at $n = 56$ because the satellites were computed only up to there (Section 3.4), and no claim is made that the sequence is finite.

For the lower rotation number, the satellite curves for $n = 13$ to 20 never reached $\theta = 0$ and many of those for $n \leq 12$ were stopped by a limit; the lower curves for $n \geq 21$ were not run (details in Online Resource 1, A.19). The limits of the method are listed in Online Resource 1, A.1. A stop at a limit gives no result and says nothing about the curve beyond it. The collapse of the step in one sense of the continuation ($n \geq 16$ in class C, $n \geq 15$ in class I) was not investigated; whether it is a fold, a collision or a secondary bifurcation is unknown. Satellites with rotation number j/n and $j > 1$ were followed from 21 members; 12 of the 33 zeros reached have a weak or failed closure (Section 2.4) and are not part of the sequence (Online Resource 1, A.19).

6.2 Numerical and theoretical limits

The continuation and the first zeros are in double precision, with the rotation at the zero between 6×10^{-12} and 4×10^{-10} turns; the orbits are then refined in multiple precision and stored with 30 digits (Section 2.4). The branch points for large n rest on singular values with a relaxed repeat tolerance, and the end orbits are checked independently of it (Online Resource 1, A.3 and A.19). Stability is spectral (linear) stability: only the multipliers were computed. They are computed in multiple precision with error estimates from two precisions for the class C orbits of $n = 5$ to 12, in one precision for the other end orbits of $n \leq 20$, and in double precision for the other orbits (Online Resource 1, A.4 and A.19); no interval arithmetic was used, and the long runs of 10,000 periods do not prove stability for longer times. The multipliers close to the branch point cannot be read in double precision and were not used: along the curves the resonant pair is classified only from a later path length (the numbers are in Section 3.3), and the types along the curves are those of a double precision continuation, checked against multiple precision at the end orbits and at the zeros only (Online Resource 1, A.13). For $n = 5$ the comparison of the two curves written

down before the run was undecided, and "different" rests on checks added after the data were seen (Section 3.3, Online Resource 1, A.12).

The split of the resonant pair at the end orbits, its absence along the curves for $n \geq 6$ and the pairing of a stable and an unstable end orbit for $n = 5$ to 12 only are numerical results and not consequences of Meyer's theorem on period-k bifurcations, which does not apply directly to the four-dimensional reversible map here (Section 3.3). The general theory of subharmonic bifurcation in time-reversible systems is developed by Vanderbauwhede (1986); a detailed comparison with the present results is not attempted here. The half-period symmetry of R and the isosceles symmetry that follows from it are properties found on the stored orbits and not derived from the equations; the lemma quoted in Section 2.1 relates the two symmetries and does not show that R has them. Why the resonant pair changes type along the curves was not examined and is open, as is the dip of the rotation angle along them (Section 4.3). The relation of Hénon is verified numerically on the stored curves and not derived again; the dip of the rotation angle, which sets δ_n, is not explained, and B is an empirical relation fitted on 13 values, not derived. At large n the members of R at which the satellites branch are near-hierarchical, with a tight binary of bodies 1 and 2 (the numbers are in Online Resource 1, A.19), and $\nu = 1/n$ is then close to an n:1 commensurability of the inner and outer motions (Online Resource 1, A.19); whether the satellite curves correspond to resonant families of the planetary-type three-body problem (see e.g. Hadjidemetriou 1976) was not examined.

6.3 Novelty and sources

No expert has confirmed that these orbits are unknown. "Not found in the sources checked" says nothing about whether an orbit is known; part of the sequence was found before (Section 5). The sources checked are listed in Online Resource 1 (A.18): the Three Body Orbits atlas, the Šuvakov gallery, the tables of Davoust and Broucke (1982), of Janković et al. (2020) and of Li et al. (2025), and the statements on the direct branch of the papers named in Sections 1.3, 1.4 and 5.4. The 2025 review of Li and Liao (2025) was read; in its passages on the satellites of the BHH family it names Janković and Dmitrašinović (2016) and Janković et al. (2020) for equal masses and Liao et al. (2022) for varying masses, and it refers to the databases three-body.ipb.ac.rs and github.com/sjtu-liao/three-body. The public listing of the second (viewed on 17 October 2026; Online Resource 1, A.18) holds, in `roadmap/Data`, four data files of BHH satellites with various masses; whether these files hold equal-mass orbits with non-zero angular momentum was not examined. The live pages of three-body.ipb.ac.rs were not checked beyond the archived copies. The literature search of 2026-10-11 (Online Resource 1, A.18) does not cover later papers, papers that do not use the words searched, or non-English literature beyond three abstracts. Several further reviews and papers that may be related could not be obtained and were not checked.

7 Data and code

7.1 Repository and supplement

The code and data are in `github.com/Utshob-k/orbit-hunter`, tag `v0.2.33-corrected` (version 0.2.33, commit ac1b1d7), licence CC-BY-4.0. The code and the data are archived on Zenodo (version DOI 10.5281/zenodo.23453312). The repository does not contain the atlas catalogue or the table of Li et al. (2025); the comparison tools read them from files given on the command line. The supplement `data/supplement-initial-conditions.json` gives the initial conditions of the 52 orbits of class C and of the 16 orbits of class I ($n = 5$ to 20) with 30 digits.

7.2 Where the orbits are

The files that hold the orbits, the start formats and the commands are listed in Online Resource 1 (A.6 and A.11) and in `docs/reproducing.md`. The short checks quoted in Sections 2.1, 3.1 and 3.2, and the files of the multipliers, are listed there too.

Supplementary information. Online Resource 1 (ESM_1.pdf): procedure details, declared changes, secondary numbers, Tables S1 and S2.

Acknowledgements. The author thanks Marija Janković for a copy of her MSc thesis and for the paper of Hénon (1977).

Statements and Declarations

Competing interests. The author has no competing interests to declare that are relevant to the content of this article.

Funding. The author declares that no funds, grants or other support were received during the preparation of this manuscript.

Data and code availability. The code and the data (Kandel 2026) are in the GitHub repository github.com/Utshob-k/orbit-hunter, tag `v0.2.33-corrected` (commit ac1b1d7); the initial conditions of the orbits are in the supplement file `data/supplement-initial-conditions.json` of the repository, and the procedure details are in Online Resource 1. The version archived on Zenodo has the DOI 10.5281/zenodo.23453312.

References

Birkhoff, G.D., Lewis, D.C.: On the periodic motions near a given periodic motion of a dynamical system. Annali di Matematica Pura ed Applicata (4) **12**, 117–133 (1934) https://doi.org/10.1007/BF02413852

Broucke, R.: On relative periodic solutions of the planar general three-body problem. Celestial Mechanics **12**, 439–462 (1975) https://doi.org/10.1007/BF01595390

Davoust, E., Broucke, R.: A manifold of periodic orbits in the planar general three-body problem with equal masses. Astronomy and Astrophysics **112**, 305 (1982)

Devaney, R.L.: Reversible diffeomorphisms and flows. Transactions of the American Mathematical Society **218**, 89–113 (1976) https://doi.org/10.1090/S0002-9947-1976-0402815-3

Dmitrašinović, V., Hudomal, A., Shibayama, M., Sugita, A.: Linear stability of periodic three-body orbits with zero angular momentum and topological dependence of Kepler's third law: a numerical test. Journal of Physics A: Mathematical and Theoretical **51**, 315101 (2018) https://doi.org/10.1088/1751-8121/aaca41

Doedel, E.J., Paffenroth, R.C., Keller, H.B., Dichmann, D.J., Galán-Vioque, J., Vanderbauwhede, A.: Computation of periodic solutions of conservative systems with application to the 3-body problem. International Journal of Bifurcation and Chaos **13**, 1353–1381 (2003) https://doi.org/10.1142/S0218127403007291

Galán, J., Muñoz-Almaraz, F.J., Freire, E., Doedel, E., Vanderbauwhede, A.: Stability and bifurcations of the figure-8 solution of the three-body problem. Physical Review Letters **88**, 241101 (2002) https://doi.org/10.1103/PhysRevLett.88.241101

Hadjidemetriou, J.D.: The stability of periodic orbits in the three-body problem. Celestial Mechanics **12**, 255–276 (1975) https://doi.org/10.1007/BF01228563

Hadjidemetriou, J.D.: Families of periodic planetary-type orbits in the three-body problem and their stability. Astrophysics and Space Science **40**, 201–224 (1976) https://doi.org/10.1007/BF00651199

Hénon, M.: Families of periodic orbits in the three-body problem. Celestial Mechanics **10**, 375–388 (1974) https://doi.org/10.1007/BF01586865

Hénon, M.: A family of periodic solutions of the planar three-body problem, and their stability. Celestial Mechanics **13**, 267–285 (1976) https://doi.org/10.1007/BF01228647

Hénon, M.: A relation in families of periodic solutions. Celestial Mechanics **15**, 99–105 (1977) https://doi.org/10.1007/BF01229050

Hristov, I., Hristova, R.: An efficient approach for searching three-body periodic orbits passing through Eulerian configuration. Astronomy and Computing **49**, 100880 (2024) https://doi.org/10.1016/j.ascom.2024.100880

Hristov, I., Hristova, R., Dmitrašinović, V., Tanikawa, K.: Three-body periodic collisionless equal-mass free-fall orbits revisited. Celestial Mechanics and Dynamical Astronomy **136**, 7 (2024) https://doi.org/10.1007/s10569-023-10177-w

Janković, M.R., Dmitrašinović, V.: Angular momentum and topological dependence of

Kepler's third law in the Broucke–Hadjidemetriou–Hénon family of periodic three-body orbits. Physical Review Letters **116**, 064301 (2016) https://doi.org/10.1103/PhysRevLett.116.064301

Janković, M.R., Dmitrašinović, V., Šuvakov, M.: A guide to hunting periodic three-body orbits with non-vanishing angular momentum. Computer Physics Communications **250**, 107052 (2020) https://doi.org/10.1016/j.cpc.2019.107052

Kandel, U.: Orbit Hunter: a search for periodic orbits of the planar three-body problem. Version v0.2.33-corrected. Zenodo. Source code: https://github.com/Utshob-k/orbit-hunter (2026). https://doi.org/10.5281/zenodo.23453312

Li, X., Liao, S.: More than six hundred new families of Newtonian periodic planar collisionless three-body orbits. Science China Physics, Mechanics & Astronomy **60**, 129511 (2017) https://doi.org/10.1007/s11433-017-9078-5

Li, X., Liao, S.: A review on periodic orbits of the general planar three-body problem. Science China Physics, Mechanics & Astronomy **68**, 289501 (2025) https://doi.org/10.1007/s11433-024-2686-6

Li, X., Tao, Y., Li, X., Liao, S.: A numerical scheme to obtain periodic three-body orbits with finite angular momentum. New Astronomy **119**, 102407 (2025) https://doi.org/10.1016/j.newast.2025.102407

Liao, S., Li, X., Yang, Y.: Three-body problem — from Newton to supercomputer plus machine learning. New Astronomy **96**, 101850 (2022) https://doi.org/10.1016/j.newast.2022.101850

Meyer, K.R.: Generic bifurcation of periodic points. Transactions of the American Mathematical Society **149**, 95–107 (1970) https://doi.org/10.1090/S0002-9947-1970-0259289-X

mpmath: a Python library for arbitrary-precision floating-point arithmetic. http://mpmath.org. Version 1.4.1. Accessed 13 October 2026

Muñoz-Almaraz, F.J., Freire, E., Galán, J., Doedel, E., Vanderbauwhede, A.: Continuation of periodic orbits in conservative and Hamiltonian systems. Physica D **181**, 1–38 (2003) https://doi.org/10.1016/S0167-2789(03)00097-6

Muñoz-Almaraz, F.J., Freire, E., Galán-Vioque, J., Vanderbauwhede, A.: Continuation of normal doubly symmetric orbits in conservative reversible systems. Celestial Mechanics and Dynamical Astronomy **97**, 17–47 (2007) https://doi.org/10.1007/s10569-006-9048-3

Rein, H., Liu, S.-F.: REBOUND: an open-source multi-purpose N-body code for collisional dynamics. Astronomy & Astrophysics 537, A128 (2012) https://doi.org/10.1051/0004-6361/201118085

Rein, H., Spiegel, D.S.: IAS15: a fast, adaptive, high-order integrator for gravitational dynamics, accurate to machine precision over a billion orbits. Monthly Notices of the Royal Astronomical Society **446**, 1424–1437 (2015) https://doi.org/10.1093/mnras/stu2164

Rimmer, R.: Generic bifurcation from symmetric fixed points of involutory area preserving maps. Bulletin of the Australian Mathematical Society **21**(1), 147–148 (1980) https://doi.org/10.1017/S0004972700011370

Šuvakov, M., Dmitrašinović, V.: Three classes of Newtonian three-body planar periodic orbits. Physical Review Letters **110**, 114301 (2013) https://doi.org/10.1103/PhysRevLett.110.114301

The Three Body Orbits atlas. https://threebodyorbits.com. Catalogue generated 2026-09-27. Accessed 9 October 2026

Vanderbauwhede, A.: Bifurcation of subharmonic solutions in time-reversible systems. Zeitschrift für angewandte Mathematik und Physik (ZAMP) **37**, 455–478 (1986) https://doi.org/10.1007/BF00945425

Supplementary Files

This is a list of supplementary files associated with this preprint. Click to download.

- ESM1.pdf